Phenylboronic acid-modified magnetic nanoparticles as a platform for carbon dots conjugation and doxorubicin delivery

Mochamad Zakki Fahmi,[1,2] Jem-Kun Chen,[3] Chih-Ching Huang,[4] Yong-Chien Ling,[5] Jia-Yaw Chang[1]*

1. Department of Chemical Engineering, National Taiwan University of Science and Technology, Taiwan, Republic of China
2. Department of Chemistry, Airlangga University, Indonesia
3. Department of Materials Science and Engineering, National Taiwan University of Science and Technology, Taiwan, Republic of China
4. Institute of Bioscience and Biotechnology and Center for Marine Bioeneironment and Biotechnology, National Taiwan Ocean University, Taiwan, Republic of China
5. Department of Chemistry, National Tsing Hua University, Taiwan, Republic of China

E-mail: jychang@mail.ntust.edu.tw

Department of Chemical Engineering, National Taiwan University of Science and Technology, 43, Section 4, Keelung Road, Taipei 10607, Taiwan, Republic of China

Phone: +886-2-27303636

Fax: +886-2-27376644

Abstract

We describe the preparation of phenylboronic acid-modified magnetofluorescent nanoparticles (NPs) consisting of $MnFe_2O_4$ magnetic NPs conjugated to fluorescent carbon dots (Cdots). These NPs are useful for both optical and magnetic resonance imaging (MRI) modalities and could also be used to deliver the water-insoluble chemotherapy drug, doxorubicin (Dox). In this study, hydrophobic $MnFe_2O_4$ NPs were transferred from organic media to water by coordinating with 4-carboxyphenylboronic acid ligands, which also act as a cancer cell-specific targeting ligand and a site for conjugation to fluorescent Cdots, allowing the preparation of phenylboronic acid-modified magnetofluorescent NPs. The NPs displayed colloidal stability at different pH values and salt concentrations, and exhibited negligible cytotoxicity against HeLa cancer cells with >85% cell viability at concentrations of up to 500 μg/mL. Confocal laser scanning microscopy showed the specificity of the magnetofluorescent NPs in HeLa cells. MRI experiments showed that the magnetofluorescent NPs were effective contrast enhancement agents in T_2-weighted MRI. Moreover, the NPs were also found to be effective fluorescent markers in an *in vivo* experiment in zebrafish embryos. Dox was attached to the NPs by π-π stacking interactions, and was delivered in a targeted manner. The results indicated that these magnetofluorescent NPs could deliver Dox efficiently and induced an anticancer effect in HeLa cells, as confirmed by confocal laser scanning microscopy and *in vitro* cytotoxicity assays.

1. Introduction

The design and synthesis of multimodal contrast agents for biomedical and clinical applications has attracted increasing interest.[1–3] Since every imaging modality has its own advantages and limitations, the development of multimodal imaging allows the merits of different modalities to be combined and increases both the accuracy and the amount of information that is available to diagnose diseases. One of the most attractive imaging modalities is dual-mode fluorescent-magnetic resonance imaging because it involves two complementary techniques. Magnetic resonance imaging (MRI) is a non-invasive diagnostic technique and offers excellent spatial resolution, deep tissue penetration, and tomographic capabilities for *in vivo* imaging; however, optical imaging affords the best sensitivity and spatial resolution for *in vitro* imaging.[4–7]

Superparamagnetic nanoparticles (NPs) are of interest as contrast enhancement agents for T_2-weighted MRI because they can dramatically shorten the transverse relaxation time (T_2) of neighbouring protons, and offer a negative contrast (dark signal) image.[8,9] Compared to organic dyes and quantum dots (QDs), which contain toxic heavy metal elements, carbon dots (Cdots) represent a new class of fluorescent nanomaterial and have many fascinating properties such as highly stable photoluminescence, low photobleaching, excellent biocompatibility, and excitation-dependent emission spectra.[10–13] To develop high-performance dual-modality magnetofluorescent contrast agents, it is necessary to design a nanostructure that contains both superparamagnetic NPs and Cdots.

Tumour-specific imaging is vital for medical diagnosis and therapy. Actively targeted NPs can efficiently deliver contrast agents directly to the target cells. The use of multiple-modality nanoprobes in conjunction with active targeting will allow early diagnoses, minimize artefacts, enable significant improvements in diagnostic accuracy, and improve therapeutic effect. Sialic acid is an anionic monosaccharide that often makes up the terminal moiety of glycan chains that are overexpressed on the surfaces of many pathologic cells; importantly, these chains are only expressed to a limited extent in healthy cells. It is well known that phenylboronic acid can rapidly react with *cis*-diol containing structures such as sialic acid through the formation of boronate esters, which makes it an ideal ligand for highly efficient and selective recognition of cancer cells.[14–16] For example, Liu and co-workers reported a phenylboronic acid-modified QD that could be used to specifically label and track the sialic acid groups on live cells.[16] Several groups also reported the use of phenylboronic acid derivatives in treatments for human immunodeficiency virus (HIV).[17,18] In addition to its high affinity and selectivity for sialic acid, phenylboronic acid is especially suitable as a targeting ligand since it is nontoxic, has relatively high stability, low immunogenicity, is inexpensive, and is easy to prepare. These properties make phenylboronic acid a superior tumour-targeting moiety for use in actively targeted nanoparticles.

In this study, we designed magnetofluorescent NPs, consisting of $MnFe_2O_4$ magnetic nanoparticles (MNPs) and fluorescent Cdots. They could be further functionalized with doxorubicin (Dox) for use as drug carriers. In order to disperse the $MnFe_2O_4$ MNPs in aqueous solution, a phase transfer approach was used and involved 4-carboxyphenylboronic acid (CBBA) ligand exchange on the surface of the $MnFe_2O_4$ MNPs. CBBA also contains a phenylboronic acid moiety, which can be used as both a cancer-specific targeting ligand and a site for the conjugation of fluorescent Cdots. The targeting specificity of the phenylboronic acid-modified magnetofluorescent NPs toward HeLa cells was evaluated using confocal microscopy and T_2-weighted MR imaging. Additionally, the magnetofluorescent NPs could bind to the water-insoluble,

chemotherapeutic drug, Dox *via* a π-π interaction with the Cdots component of the NPs. *In vitro* investigations to assess its potential theranostic applications in HeLa cervical cancer cells were carried out using confocal laser scanning microscopy (CLSM), T_2-weighted magnetic imaging, and transmission electron microscopy (TEM). Finally, *in vivo* observation using zebra fish (*Danio rerio*) embryos confirmed the cytotoxicity profile of the NPs, and CLSM was used to track the NPs in the embryo.

2. Experimental Section

2.1 *Materials*

3-(4,5-dimethylthiazol-2-yl)-2,5-diphenyltetrazolium bromide (MTT, 97.5%), iron (III) acetylacetonate (Fe(acac)3, 97%), osmium tetraoxide (4%), α(2→3,6,8,9) neuraminidase (sialidase), and agarose were purchased from Sigma-Aldrich (Milwaukee, WI, USA). Glutaraldehyde (25%), manganese (II) acetylacetonate (Mn(acac)2, 98%), 4-Carboxy-3-chlorobenzeneboronic acid (CBBA, 97%) were purchased from Alfa-Aesar (Ward Hill, MA, USA). FA (>98%) was purchased from T.C.I. Chemical Co. (TCI, Japan). Oleylamine (80-90%), tricaine methanesulfonate, and benzyl ether (99%) were purchased from Acros Organics (Geel, Belgium). Sodium hydroxide and citric acid anhydrous (CA) were purchased from Showa Kako Corp. (Osaka, Japan). Dox was purchased from Fusol Material Co., Ltd. (Tainan, Taiwan). Dimethyl sulfoxide (HPLC grade) was purchased from Scharlau (Barcelona, Spain). All chemicals were used directly without further purification.

2.2. *Preparation of MNPs and CBBA-MNPs (CM)*

To prepare oil-soluble $MnFe_2O_4$ MNPs, Fe(acac)$_3$ (2 mmol) and Mn(acac)$_2$ (1 mmol) were completely dissolved in a mixture of benzyl ether (15 mL) and oleylamine (15 mL), and heated at 110 °C for 1 h under argon flow. The temperature was then increased to 300 °C, left for 1 h, and then cooled to room temperature. The resulting MNPs were washed with ethanol twice and precipitated by centrifugation (6000 rpm, 10 min).

Ligand exchange was then carried out to obtain water-soluble $MnFe_2O_4$ MNPs. MNPs (10 mg) were dissolved in chloroform (300 μL), and this solution was gradually added to a solution of CBBA in ethanol (10 mL; 15 mg/mL). The combined solution was then sonicated for 5 min using an ultrasonic probe (VCX 130 PB, 130 W, 20 kHz, Sonics and Materials Inc., Newton, CT). Excess hexane was then added to precipitate the ligand-exchanged MNPs. After decanting the solvent and washing with ethanol to remove excess CBBA, the resulting CBBA-MNPs (CM) were dissolved in DI water for use in experiments.

2.3. *Preparation of Cdots*

Cdots were prepared by pyrolyzing CA according to a previously published procedure with some modification.[19] Briefly, CA (200 mg) was calcined at 240 °C for 30 min. This process turned the CA orange owing to carbonization and the generation of graphitic nanostructures. After cooling to room temperature, NaOH solution (0.5 M) was added until the pH of the solution was neutral. A centrifugal filter unit with a molecular-weight cut off (MWCO) of 1000 Da was then used to narrow the size distribution of the Cdots and remove small molecules. On average, 70 mg Cdots were obtained from 200 mg CA.

2.4 *Preparation of Cdot-CM conjugates (CCM) and Dox loading*

To conjugate Cdots to the surface of CM, Cdots (5 mg) were mixed with CM solution (5 mL; 4 mg/mL) and ultrasonicated (VCX 130 PB, 130 W, 20 kHz, Sonics and Materials Inc., Newton, CT) for 1 min. The

solution was subsequently dialyzed with a high-flow ultrafiltration membrane (MWCO 3500 Da; Cellu Sep H1, Orange Scientifique, Belgium) for 24 h to remove unconjugated Cdots from the solution.

To prepare Dox-loaded CCM (DCCM), Dox solution (100 μL; 1 mg/mL) was added to CCM solution and vigorously stirred at 65 °C for 5 h. After this time, the solution was dialyzed for 24 h using a membrane (MWCO 3500 Da; Cellu Sep H1, Orange Scientifique, Belgium) to remove the free DOX from the DCCM solution. The concentration of Dox in DCCM was determined by measuring the absorption of the samples at 482 nm and comparing to a standard calibration curve. Dox loading efficiency (LE) and loading amount (LA) were calculated using equations (1) and (2).

$$\text{Loading Efficiency} \, (\%) = \frac{\text{mass of Dox in DCCM}}{\text{mass of Dox in feed}} \times 100\% \qquad (1)$$

$$\text{Loading Amount} \, (\%) \;\; = \frac{\text{mass of Dox in DCCM}}{\text{mass of DCCM}} \times 100\% \qquad (2)$$

2.5. *In vitro cytotoxicity study*

The *in vitro* cytotoxicity of the NPs was investigated in HeLa cancer cells using the MTT assay. HeLa cells were seeded in a 12-well plate at 25,000 cells per well and left for 24 h. The cells were then washed with phosphate-buffered saline (PBS) and incubated with various concentrations of sample for 24 h. After washing the plate twice with PBS, MTT reagent (1 mL 500 mg/mL) was added, and the cells were incubated for 4 h. After carefully removing the liquid, dimethyl sulphoxide (1 mL) was added to each well to dissolve the dark-blue formazan crystals. The absorbance of formazan at 570 nm was measured by using a Biotech Powerwave XS plate reader. The amount of formazan generated by the cells is proportional to the number of live cells.

2.6. *Bio-TEM imaging*

Cells were seeded in a plate containing culture medium (2 mL) and incubated for 24 h. After this time, CCM (300 μL) was added, and the cells were incubated for a further 1 h. Cells with internalized nanoparticles were washed with PBS, trypsinized, centrifuged, and re-washed with PBS. The cells were then fixed once with 0.2% glutaraldehyde at 4 °C for 5 min and then twice with 1% glutaraldehyde at 4 °C for 60 min. After washing with PBS, the cells were stained with 1% osmium tetraoxide for 60 min and re-washed with PBS. A series of increasingly concentrated ethanol solutions (50%, 70%, 80%, 90%, 95%, and 100%) was used to dehydrate the cells; ethanol solution was added, left for 15 min before being replaced with the next most concentrated solution. Epoxy resin, consisting of cycloaliphatic epoxide resin (ERL 4221; 1 g), nonenyl succinic anhydride (NSA; 2.6 g), DER-736 epoxy resin (0.6 g), and 2-(dimethylamino) ethanol (DMAE; 0.2 g), was then added to the dehydrated cells, and they were then placed in an oven at 60 °C for 48 h. Ultra-thin sections of approximately 80 nm thickness were cut with diamond knives using an ultramicrotome (Leica Microsystems, Germany) and transferred to 200-mesh copper grids. The images were examined using a Tecnai G2 F20 TEM microscope (Philips, Holland).

2.7 *In vitro CLSM imaging*

HeLa cells were seeded in a plate containing culture medium (2 mL) and incubated for 24 h. After this time, sample (300 μL) was added and following 60 min incubation, the cells were washed three times with PBS and then fixed with 70% alcohol for 10 min. Fluorescence images of the HeLa cells were acquired using an

inverted confocal microscope (Leica TCS SP2, Leica Microsystems) equipped with a 63 × 1.32 NA oil immersion objective. Confocal images were obtained by illuminating the samples with the inline Ar (488 nm) and He-Ne (503–680 nm and 588 nm) lasers.

2.8 *In vitro MRI*

HeLa cells were seeded in a plate, and medium (approximately 2 mL) was added. The cells were then incubated for 24 h. After this time, the medium was replaced with fresh medium (2 mL) containing CCM at different concentrations, and the cells were incubated for 24 h. After this time, the cells were washed with PBS, trypsinized, centrifuged, re-suspended in PBS (1 mL), and placed in 1.5-mL tubes for MRI. T_2-weighted MRI was performed using a Bruker MedSpec 7 T whole-body system (Ettlingen, Germany) with a birdcage head coil.

2.9 *In vivo cytotoxicity study and CLSM imaging*

An *in vivo* cytotoxicity study was carried out using embryonic zebra fish, which were generated from healthy female and male zebra fish. The fish were kept under laboratory conditions at 25 °C with a 14 h light/10 h dark cycle in an aquarium containing water, which was purified by reverse osmosis and supplemented with a commercially available salt solution. After fertilization, the embryos were collected and rinsed several times with oxygenated water. Then, a stereomicroscope was used to collect healthy embryos and seeded onto a 96-well plate. Various concentrations of CCM, which had been diluted with oxygenated water, were added to the embryos and replaced every day. The embryos were examined every 24 h for 5 days using an inverted microscope (Olympus IX70, Olympus America, Melville, NY) to assess embryo mortality, hatching rate, and morphological abnormalities.

On the fifth day, embryos that had been treated with CCM were removed from the plate in oxygenated water and anaesthetized by adding 1 drop of tricaine (15.6 M). The unconscious embryo was then mounted in low melt agarose (2% w/v) and imaged using an inverted confocal microscope (Leica TCS SP2, Leica Microsystems) with the inline Ar (488 nm) laser to track the emission of Cdots in the embryo.

The use of animals in experiments was reviewed and approved by the Animal Experimentation Committee of National Tsing Hua University.

2.10 *Characterization*

TEM samples were prepared by dropping a dilute solution of nanoparticles onto 200-mesh copper grids coated with a thin Formvar-carbon film and allowing the solvent to evaporate in air at room temperature. High-resolution TEM (HR-TEM) imaging and selected area electron diffraction (SAED) images were recorded using Philips Tecnai G2 F20 microscope (Philips, Holland), equipped with an energy dispersed X-ray spectroscopy (EDS) detector with an accelerating voltage of 200 kV. X-ray powder diffraction (XRD) patterns were obtained using a Rigaku 18 kW rotating anode source X-ray diffractometer with the Cu Kα1 line (λ = 1.54 Å). UV-vis absorption spectra were measured using a JASCO V-670 spectrometer. Fluorescence spectra were recorded using a JASCO FP-6500 spectrofluorometer equipped with a 150 W xenon lamp. MRI was performed using a Bruker MedSpec 7 T whole-body system (Ettlingen, Germany) with a birdcage head coil, to estimate the transverse relaxation time (T_2) for each sample, coronal images (slice thickness = 2 min) were acquired at various echo times (TE) from 11 to 77 ms with a repetition time (TR) of 5000 ms. The magnetic properties of the nanoparticles were measured using a superconducting quantum

interference device (SQUID) magnetometer (Magnetic Property Measurement System 5S, Quantum Design) with maximum applied field up to 10 kOe at room temperature.

3. Results and discussion

The entire procedure used to prepare magnetofluorescent NPs for use as high-performance optical/MR dual-modality molecular imaging contrast agents and drug carriers is illustrated in Scheme 1. First, oleylamine-stabilized $MnFe_2O_4$ MNPs were prepared using a solvothermal synthetic route. Subsequently, oleylamine-stabilized $MnFe_2O_4$ MNPs were converted to phenylboronic acid-capped $MnFe_2O_4$ MNPs (CM) using ultrasonic-assisted CBBA ligand exchange. CBBA was chosen as a capping ligand because it contains carboxylate groups, which can coordinate to the surface of $MnFe_2O_4$ MNPs and enable convenient phase transfer of MNPs from organic solvents into aqueous solutions (Scheme 1(a)). Additionally, it is well known that the phenylboronic acid moieties of CBBA can covalently bond to *cis*-diol moieties in a reversible fashion; this makes it an ideal ligand for highly efficient, selective recognition of the sialic acid groups that are overexpressed on the surface of cancer cells. Not only did the presence of phenylboronic acid groups on the surface of CM allow specific targeting of cancer cells, it also allowed the conjugation of photoluminescent Cdots through the formation of cyclic boronate esters. On the edges of Cdots, there are many hydroxyl groups that can easily form cyclic boronate ester bonds with CM (Scheme 1(b)). The resulting water-soluble Cdot-CM conjugates (CCM) have magnetofluorescent properties and are tumour-specific. To demonstrate the capability of CCM as an anticancer drug carrier, Dox was attached to the surface of CCM through π-π stacking interactions,[6,20] as shown in Scheme 1(c).

Scheme 1. Schematic illustration of (a) phase transfer process, (b) Cdot conjugation, and (c) Dox loading onto MNPs.
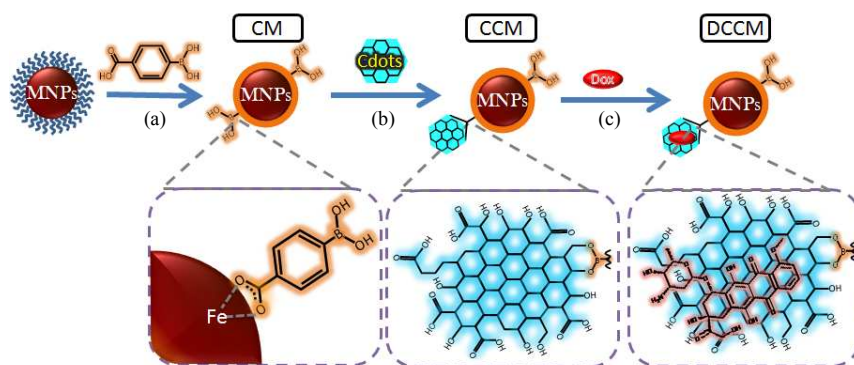
3.1 *Phase transfer of $MnFe_2O_4$ MNPs via CBBA*

$MnFe_2O_4$ MNPs were synthesized in the organic phase *via* a solvothermal method using oleylamine as a capping ligand. TEM images showed the formation of spherical MNPs with an average diameter of 10 nm (Figure 1). HR-TEM and SAED analyses of $MnFe_2O_4$ MNPs (Figures S1(a) and (b)) showed crystal lattices, and XRD analysis (Figure S1(c)) showed the presence of (311) and (004) lattice planes (JCPDF 38-0430). The elemental characterization using EDS confirmed that the NPs contained Mn, Fe, and O (Figure S1(d)). After ligand exchange, TEM images of CM showed individually dispersed NPs without significant aggregation, indicating colloidal stability in aqueous, as well as organic, solvents (Figure 1(b)).
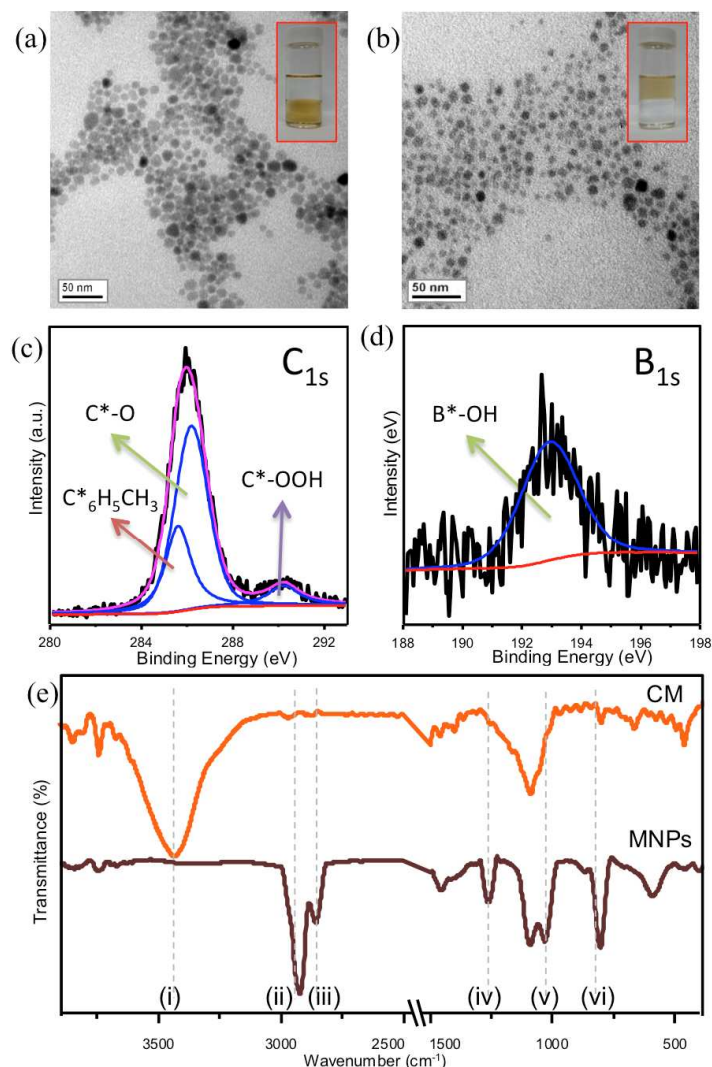
Figure 1. TEM images of pristine MnFe$_2$O$_4$ MNPs (a) and CM (b). The insets show phase transfer of MnFe$_2$O$_4$ MNPs dispersed in hexane (bottom) into water (top) after CBBA ligand exchange. XPS high-resolution data in the C1s (c) and B1s (d) regions of CM with peak-fit process using Gaussian–Lorentzian components, red line shows the designated baseline with deconvoluted peaks and overlapping peak shown as the blue and pink lines, respectively. (e) FTIR spectra of MNPs and CM.

Some amine- and carboxyl-based molecules are commonly used as capping ligands in the synthesis of MNPs because they have a high affinity for iron.[21–24] Therefore, the carboxylic groups of CBBA were able to displace oleylamine. To confirm the structure of CM, XPS analysis was carried out and focused on the binding energy ranges of carbon and boron (Figures 1(c) and (d)). The high-resolution C1s XPS spectrum of CM shows the presence of carbon signals (from benzene) at 285.1 eV, C-O functionality at 286.2 eV, and carboxylic acid groups at 290.2 eV. The significantly higher peak area for C-O as compared to carboxylic acid suggests that most of the carboxylic acid groups in CBBA were coordinated to the MNPs. The boronic acid signal on the B1s XPS spectrum remained at 193.2 eV and no new peaks appeared. This showed that CBBA had replaced the original ligand and that free boronic acid was present on the surface. Additionally, Fourier-transform infrared (FTIR) spectroscopy (Figure 1(e)) supports the above conclusions by

demonstrating that CBBA had replaced oleylamine. The FTIR spectrum of the MNPs shows the presence of oleylamine as evidenced by the C-H stretching vibrations at 2928 and 2843 cm^{-1} (ii and iii), C-C skeletal vibration at 1267 cm^{-1} (iv), and C-H bending vibrations at 1099 and 802 cm^{-1} (v and vi). The intensity of these vibrations is dramatically lower in CM and a new band at 3420 cm^{-1} (i) appears owing to the hydroxyl group in boronic acid.

To examine the magnetic properties of CM, T_2 relaxation time analysis was conducted using a 7 T MRI scanner. The T_2 relaxation rates of pristine MNPs and CM are shown in Figure 2(a), and ligand exchange was shown to slightly reduce the T_2 relaxation efficiency (r_2) from 2.239 mM^{-1}s^{-1} (MNPs) to 1.752 mM^{-1}s^{-1} (CM). As shown in the inset of Figure 2(a), the T_2-weighted image intensities of both samples decrease with increasing Fe concentration, resulting in darker images. The result suggests that this CM can be utilized as a MR contrast agent. Magnetic hysteresis data obtained using a SQUID magnetometer demonstrated the magnetic properties of CM (Figure 2(b)). The superparamagnetic nature of both MNPs and CM is shown by their saturation magnetizations, which had values below the theoretical value of magnetite (92-100 emu g^{-1}).[25] MNPs and CM achieved saturation magnetization at 23.76 emu/g and 21.32 emu/g, respectively, at 10 kOe. Moreover, the narrow hysteresis of both MNPs and CM—with coercivity values of about 1 and 5 kOe, respectively—indicated their superparamagnetic nature.[26]
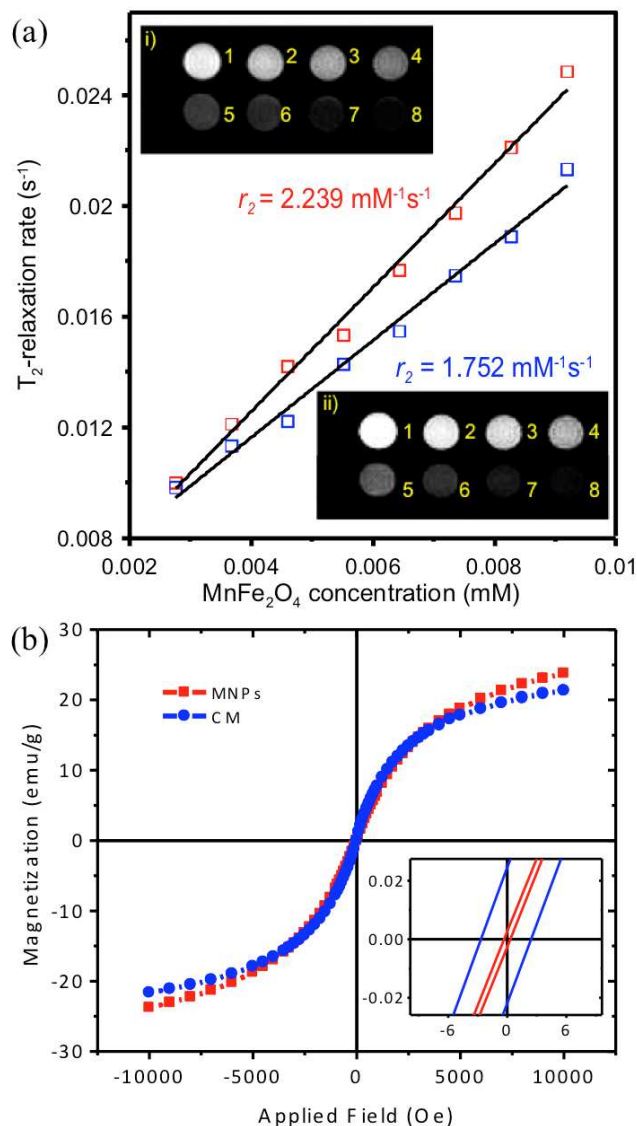
Figure 2. (a) T_2 relaxation rate of pristine MNPs (red symbol) and CM (blue symbol) as function of MNP concentration (7T, 25 °C). Insert shows T_2-weighted MR image of pristine MNP (up) and CM (bottom), the sample concentration from 1 to 8 following 0.0027, 0.0037, 0.0046, 0.0055, 0.0064, 0.0074, 0.0083, and 0.0092 mM. (b) Magnetization curves of MNP (red) and CM (blue) with magnetic hysteresis loop at low field region shown as the inset.

For NPs intended for biological applications, especially cancer detection and therapy, it is important to verify their colloidal stability at a range of biological pH values and salt concentrations. It is widely reported in the literature that physiological ionic strength is around 0.15 M and that physiological pH varies between pH 4.5 in intracellular compartments and pH 8 in the pancreas.[27] Figure 3(a) shows that CM is stable for up to 12 h at pH 3–12, and stable for up to 24 h at pH 5–12. CM precipitated at low pH because CBBA became protonated and therefore uncoordinated from the MNPs. Furthermore, the structure of CM was stable at NaCl concentrations of 0–0.5 M (Figure 3(b)) and solutions remained clear. Both stability investigations indicated that CM was stable and safe enough for biological applications.
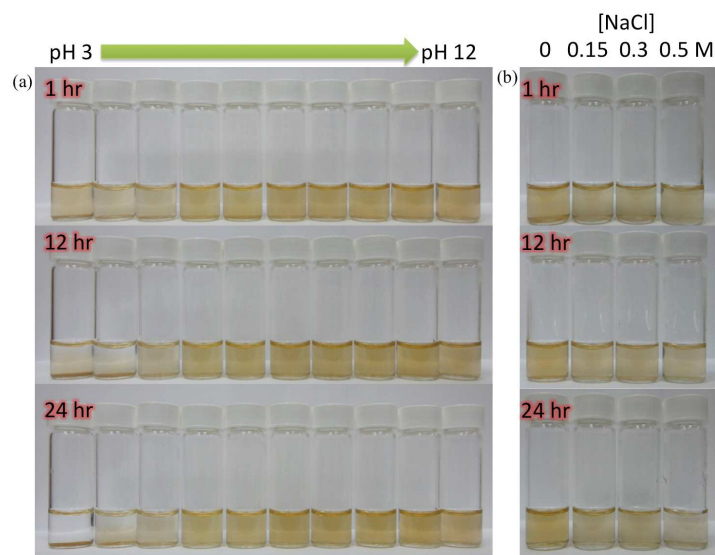
Figure 3. (a) Photographs of CM at different pH values. (b) Photographs of CM at different NaCl concentrations.

3.2 *Preparation of CCM and DCCM*

As mentioned above, we attached photoluminescent Cdots to CM. Cdots are the preferred photoluminescence agents for biological applications owing to their lack of toxicity. In this study, Cdots were prepared by pyrolyzing citric acid at 240 °C for 30 mins.[19] At such a high temperature, citric acid is dehydrated and subsequently carbonizes to form graphitic structures. By carefully adjusting the time and temperature of pyrolysis, delimited graphene structures or incomplete carbonization can be achieved, and this results in photoluminescent materials. The exact mechanism by which Cdots produce photoluminescence is yet to be confirmed; however, a mechanism involving radiative recombination and emissive trap resulting from sp^2 carbons surrounded with sp^3 carbons is currently suspected.[19,28,29] The successful preparation of Cdots was confirmed by Raman spectroscopy (Figure 4(a)). Although absent in the spectrum of citric acid, the Cdot spectrum contains a strong G-band at 1582 cm^{-1} due to the formation sp^2-hybridized carbon atoms; the higher intensity D-band at 1332 cm^{-1} indicates the presence of sp^3-hybridized carbon atoms on the edges of the Cdots. AFM demonstrated that the Cdots had a narrow size distribution and an average size of about 1.8 nm (Figure 4(b)). HR-TEM supported the AFM result by allowing direct observation of the carbon lattice (Figure 4(c)). These data suggested that Cdots with a carbon lattice structure had been obtained. Furthermore, the optical properties of Cdots were investigated using absorption and photoluminence spectroscopy (Figure 4(d)). Cdots had a broad absorption at ~360 nm, and their emission fluorescence shifted to a higher wavelength following excitation with higher wavelengths. A similar phenomenon has been reported by previous studies.[30–33]
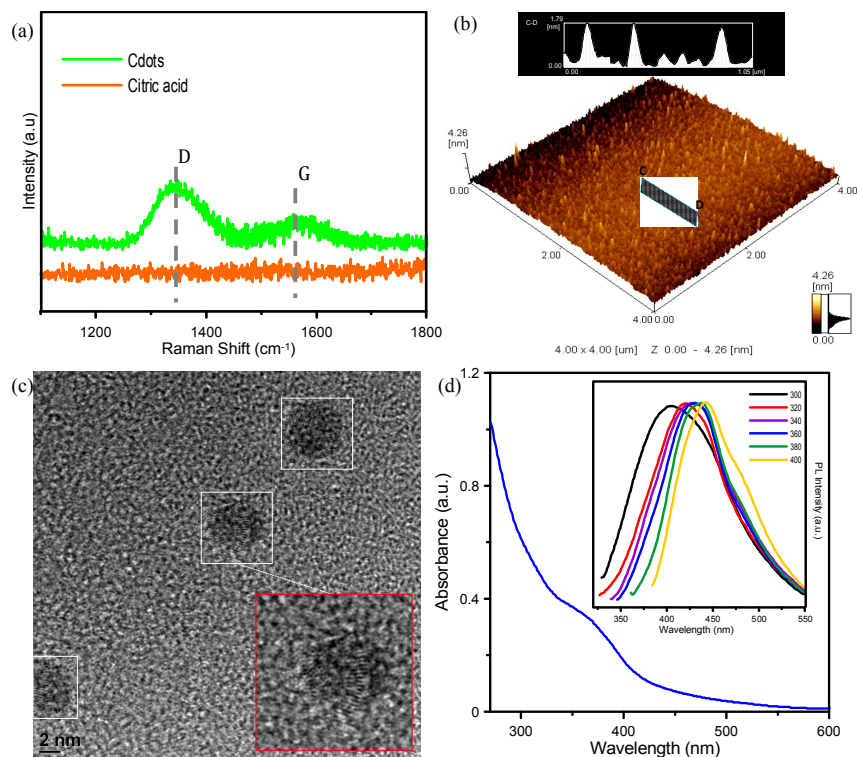
Figure 4. (a) Raman spectra of citric acid and Cdots. (b) AFM characterization of Cdots with detailed particle size in the C-D region. (c) HR-TEM images of Cdot shows carbon lattice on white box, red area show high magnification of adjusted Cdots. (d) UV-vis absorption spectra of Cdots and PL emission spectra with different excitation wavelengths shown inset.

Absorption and photoluminence spectra were recorded to prove Cdot conjugation and Dox loading. As shown in Figure 5(a), the characteristic absorption of Cdots at 360 nm can be seen in samples of both CCM and DCCM and a Dox-specific adsorption at around 485 nm can be seen in the spectrum of DCCM. The LA and LE of Dox on CCM were determined, spectroscopically, to be 2.4% and 42.5%, respectively. LA was optimized by varying Dox concentration. As shown in Figure 5(b), LA could be increased to 35% by using saturated Dox solution. CCM is a promising delivery vehicle for Dox as well as a promising imaging agent.
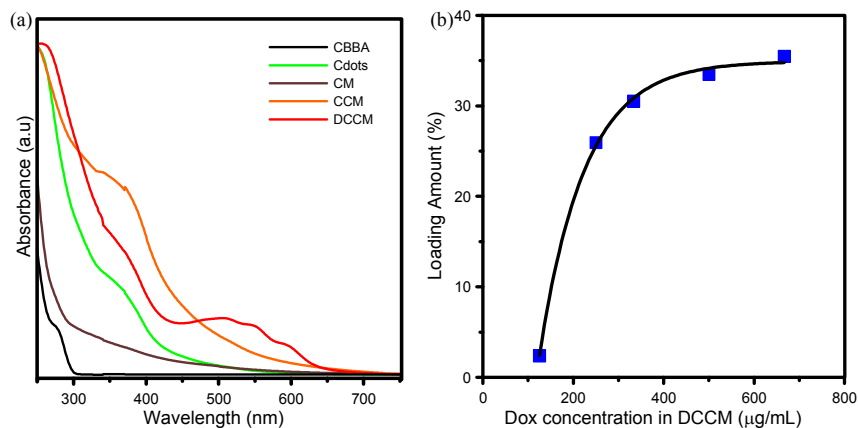
Figure 5. UV-vis absorption spectra of CBBA, Cdots, CM, CCM, and DCCM. (b) Loading amount curve of DCCM at various Dox concentrations (pH solution = 7.4).

3.3 *In vitro* optical imaging investigation

Several *in vitro* studies were carried out to investigate the effectiveness of DCCM as a cancer theranostic. CLSM was used to examine the fluorescent emission of CCM in HeLa cancer cells. HeLa cells were chosen as a model of cancer cell lines to demonstrate the specific recognition because of the abound sialic acid on the cell surface.[34-36] The excitation-dependent fluorescence of Cdots means that blue light (λ_{ex} = 488 nm) can be used and this avoids the strong background fluorescence of cells that occurs when UV laser excitation is used. As shown in Figure 6(a), strong green fluorescence was observed in CCM-treated HeLa cells after 1 h of incubation. The green fluorescence appears in the cytoplasm of HeLa cells, indicating that CCM enters cells *via* glycoprotein receptor-mediated endocytosis. For comparison, HeLa cells were also incubated with free, unmodified Cdots, which contained no phenylboronic acid. Examination of the Cdot-treated cells showed no significant green fluorescence (Figure 6(b)). As mentioned above, phenylboronic acid has a high affinity for glycoproteins such as sialic acid, which is over-expressed on a wide variety of pathologic cells. The above results indicated that the phenylboronic sites on CCM are able to facilitate the intracellular uptake of CCM through receptor-mediated endocytosis. Endocytosis is a general mechanism by which different extracellular materials are internalized into cells. Endocytosis is an energy-dependent uptake mechanism; therefore, the efficiency of endocytosis behaviour is reduced by low temperatures.[37-39] In order to verify whether our CCM enter cells *via* endocytosis, we incubated cells with CCM at 4 °C and analyzed them using confocal microscopy. As shown in Figure S2(a), the cellular uptake of CCM significantly decreased when the incubation was performed at 4 °C, suggesting that CCM was taken up by endocytosis. To confirm that CCM entered cells *via* glycoprotein receptor-mediated endocytosis, competition experiments were performed in the presence of 0.1 M free CBBA (Figure S2(b)). CCM treatment in the presence of free CBBA resulted in negligible intracellular fluorescence because excess free CBBA partially binds to the surface receptors of HeLa cancer cells and limits the intracellular uptake of CCM. Additionally, we incubated CCM with sialidase-treated HeLa cells. The sialidase was often acted as a cleaving agent to remove sialic acids moiety from glycoprotein of cell surfaces.[16] As expected, negligible green fluorescence signal was displayed for HeLa cells (Figure S3), which clearly suggested that the easy internalization of the CCM into HeLa is indeed through specific reconnition between CBBA targeting ligands of CCM and sialic acids on the cell surface. The suitability of CCM for use as a contrast agent was revealed by an *in vitro* T_2-weight study of HeLa cells after incubation with CCM (Figure 7(a)). The 7 T-MRI scan showed dark signals in CCM-treated HeLa cells with an intensity that was dependent on the concentration of CCM. In addition, as shown in Figure 7(b), bio-TEM confirmed the presence of well-dispersed CCM in the cytoplasm of HeLa cells.
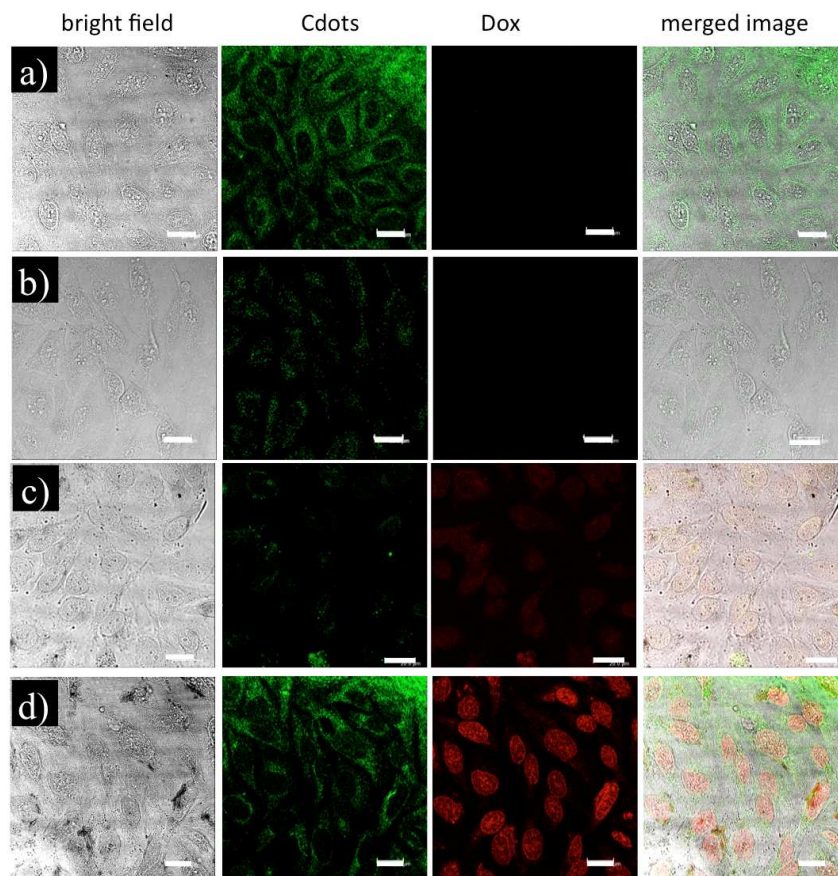
Figure 6. CLSM images of HeLa cells treated with (a) CCM and (b) free Cdots and incubated for 1 h. CLSM images of HeLa cells treated with DCCM and incubated for (c) 20 min and (d) 1 h, respectively. HeLa cells imaged by excitation at 488 nm and 546 nm to detect Cdots and Dox, respectively.

To demonstrate the suitability of CCM for use as an anticancer drug delivery carrier, Dox was attached to the surface of CCM through π-π stacking and hydrophobic interactions to give DCCM, as shown in Scheme 1(c). The subcellular localization of DCCM was investigated using confocal microscopy. HeLa cells were treated with DCCM and incubated for 20 min. As shown in Figure 6(c), only weak green and red fluorescence were detected, indicating that DCCM did not efficiently enter HeLa cells after this short incubation time. However, as shown in the second panel of Figure 6(d), after 1 h incubation, green fluorescence was well distributed within the cytoplasm indicating the entry of DCCM. This result is consistent with the cellular uptake experiments (second panel in Figure 6(a)) and suggests that our NPs are taken up by the HeLa cells *via* glycoprotein receptor-mediated endocytosis. As shown in the third panel of Figure 6(d), strong red emission signals can be seen in the nucleus of the HeLa cells. Z-slices of the CLSM images showed the exact position of DCCM and CCM in cells (Figure S4) and it was found that the red emission caused by Dox is found only in the nucleus. It is generally agreed that Dox accumulates in the nucleus before interacting with topoisomerase II and causing DNA cleavage—the mechanism responsible for its superior antitumor activity.[40] An explanation of the nuclear localization of Dox is that DCCM delivers Dox through the cell membrane *via* glycoprotein receptor-mediated endocytosis, and subsequently, Dox dissociates from DCCM in the acidic cellular environment (pH 4−6). Dox can then enter the nuclear region. The pH-sensitive Dox-release behaviour of DCCM may also be attributed the high solubility of Dox in a low-
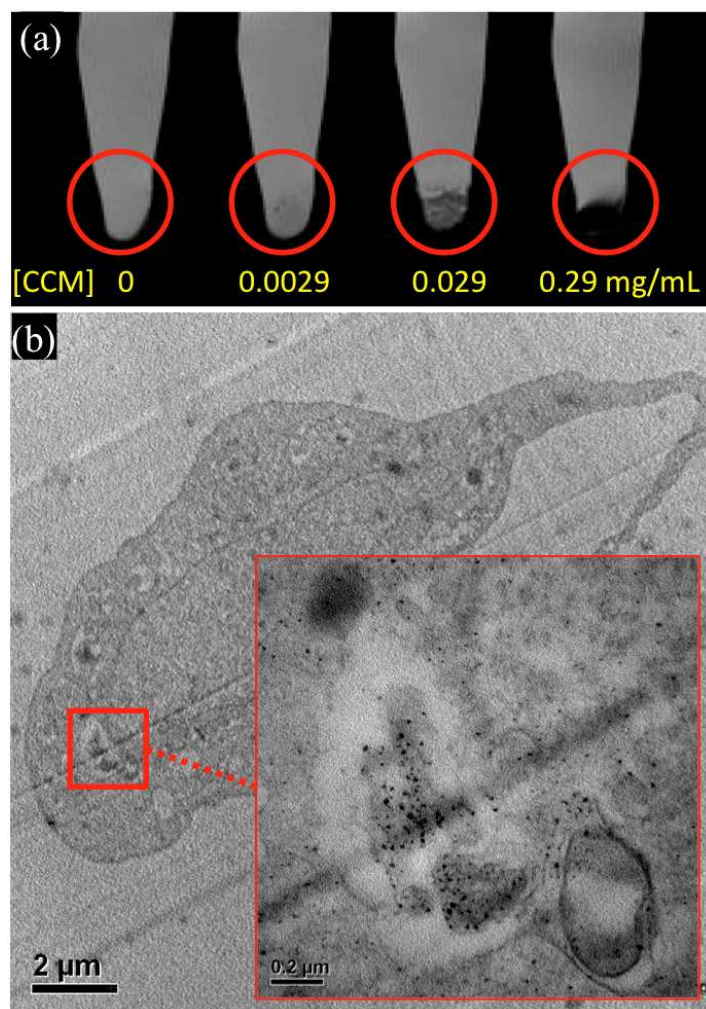
pH medium.

Figure 7. a) *In vitro* T$_2$-weighted MR image of HeLa cells treated with various concentrations of CCM and incubated for 24 h. b) Bio-TEM images showing the internalization of CCM into HeLa cells after 1 h incubation, the high-magnification image (red square) of the designated has a scale bar 0.2 μm.

3.4 *Dox release evaluation*

To get further proof of concept of the proposed pH-sensitive Dox release behaviour, we analyzed the drug release of Dox from DCCM over time, in PBS buffers with various pH values. Dialysis membrane equipment (MWCO 3500 Da) was used to observe the rate of Dox release at different pH values. As shown in Figure 8(a), the Dox release profile revealed that the release rate was pH-dependent. DCCM exhibited good stability under neutral conditions (pH 7.4) and released less than 10% of Dox in 5 h. After incubation at pH 7.4 for 72 h, about 22% of the bound Dox was released from the DCCM. However, when the pH value was adjusted to acidic condition for 72 h, ca. 75% and 60% of the DOX loaded on DCCM were released into the solution of pH 5.0 and 6.0, respectively. The amount of Dox released is enhanced at a lower pH because of the high solubility of Dox in a low-pH medium, allowing the release of a large amount of Dox from the DCCM. This property of the NPs is highly desirable and useful for drug delivery applications, because the pH value of

many tumors is one order of magnitude lower than that of normal tissues, and the tumor cells normally exhibit an acidic environment. Additionally, intracellular lysosomes and endosomes are acidic, which facilitating the Dox to release and pass through the nuclear pores to enter the cell nucleus. And this behavior thereby leads to cell death. The effect of acid on the cyclic boronate esters that connect Cdots and CM was also investigated. As mentioned above, a low pH enables the release of Dox, but also has the potential to break cyclic boronate ester bonds and destroy CCM. As previously mentioned, Cdots and Dox possess characteristic absorbances at 360 nm and 485 nm, respectively. Therefore, the pH release experiment was repeated at pH 5 except this time the filtrate was analyzed for the presence of Cdots, not PBS (Figure 8(b)). The resulting spectra show that the change in the absorption intensity 360 nm is negligible compared to the increase at 485 nm. This indicated that CCM was stable, and Cdots were not detached under acidic conditions.
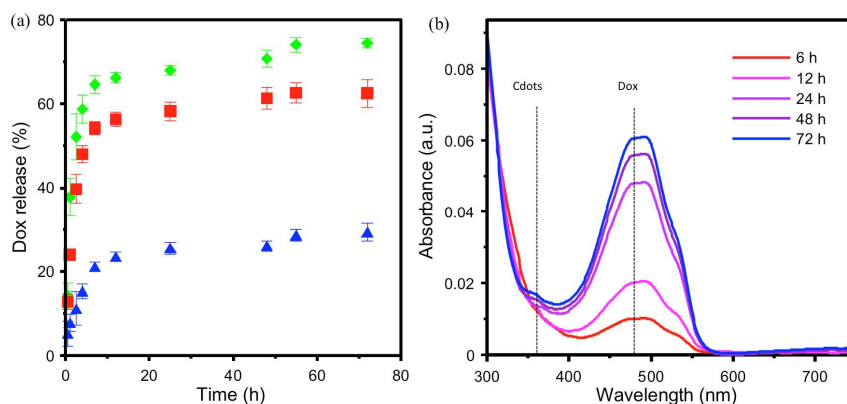

Figure 8. (a) pH-triggered release of Dox from DCCM in PBS buffer at pH 7.4 (blue), 6.0 (red), and 5.0 (green). (b) UV-vis absorption spectra of solution passing through dialysis membrane (MWCO 3500) at pH 5 to measure Dox and Cdot release from DCCM over time.

3.5 *In vitro and in vivo cytotoxicity evaluation*

To assess their suitability for future biological applications, the cytotoxicity of CM, CCM, and DCCM were evaluated using the MTT assay in HeLa cancer cells. As shown in Figure 9(a), after 24 h treatment, cell viability remained high for both CM and CMM. This suggested that the NPs have low cytotoxicity—even at concentrations of up to 400 μg/mL. The toxicity of the Dox-containing DCCM was high even at a low concentrations (10 μg/mL). The cytotoxicity of DCCM also increased over time (Figure 9(b)). This suggests that longer incubation times are needed for increased Dox activity. In addition, we compared the cytotoxicity of DCCM and free Dox using identical conditions and concentrations (based on the LA of Dox in DCCM). As shown in Figure 9(c), DCCM more effectively reduces HeLa cell viability than free Dox. The presence of CBBA is expected to be responsible for the increased efficiency of DCCM-delivered Dox. The half-maximal inhibitory concentration (IC_{50}) value was determined using the dose-response graphs obtained after treating HeLa cells with free Dox and DCCM (Figure S5). Analysis shows that free Dox has a higher IC_{50} value (153.3 μg/mL) than DCCM (78.2 μg/mL). This suggests that DCCM effectively delivers Dox to the targeted cell.

To gain a deeper insight into the cytotoxicity of the NPs, zebrafishes were treated with CCM. The use of zebrafish embryos has several advantages; they have a small size, are optically clear, undergo rapid development, are fundamentally similar to other vertebrates including humans, and are inexensive. These advantages suggest that zebrafish is a very useful vertebrate model for determining the toxicity profile of the NPs. [6, 41–43] In order to evaluate sub-lethal doses of CCM, various concentrations of CCM were used as environmental medium for culturing zebra fish eggs, which were incubated for 120 h post fertilization (hpf). Even when the concentration of CCM was 1.4 mg/mL, no mortality or malformation was observed, and the fish had a similar morphology to the untreated control fish (Figure 10). These results indicated that CCM was nontoxic and suitable for clinical applications. Moreover, *in vivo* CLSM was used to track CCM in the body of zebrafish larvae. Figure 11 clearly shows strong emission from Cdots in the brain, nervous system, and muscles of the fish embryo after 120 hpf treatment with CCM. These results suggest that CCM is safe and stable in complicated biological systems, and that it has potential as an effective fluorescence marker for *in vivo* bioimaging applications.
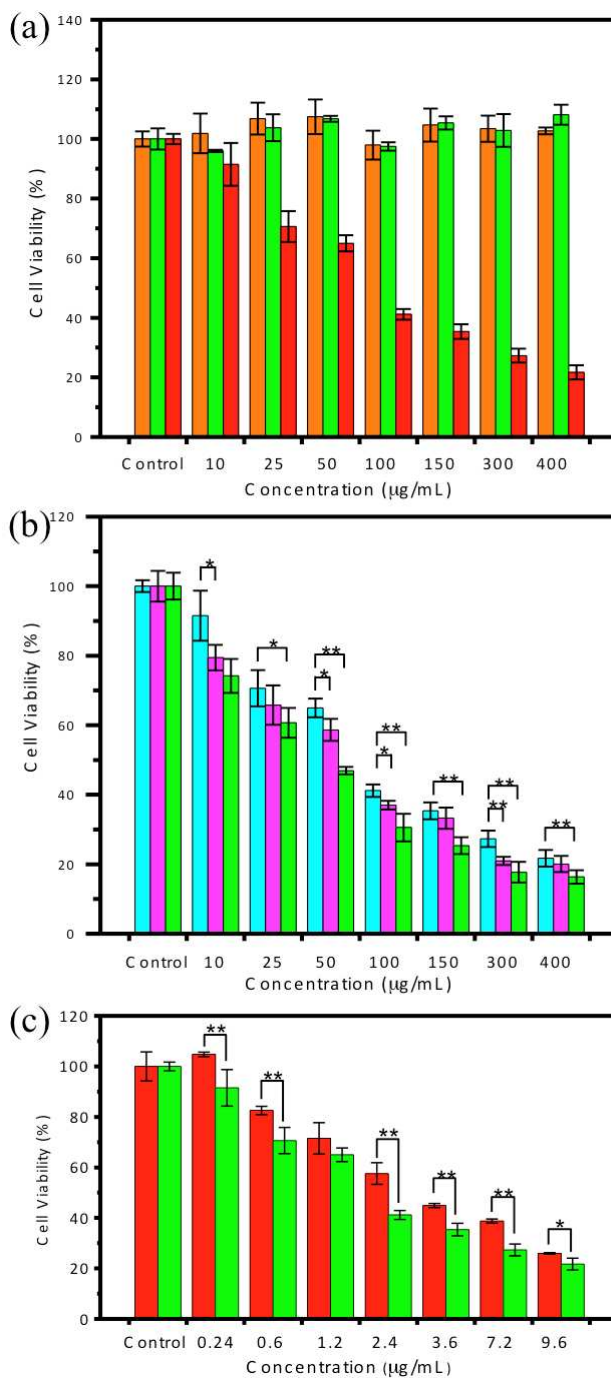
Figure 9. (a) Cell viability study using MTT assay of HeLa cells after 24 h treatment with CM (orange), CCM (green), and DCCM (red). (b) HeLa cancer cell viability after treatment with DCCM after 1 day (cyan), 2 days (magenta), and 3 days (green). (c) MTT based cell viability study of HeLa cells after 24 h treatment with DCCM (green) and free Dox (red). All MTT data are represented as mean ± SD (n = 3). *p < 0.05, **p < 0.01.
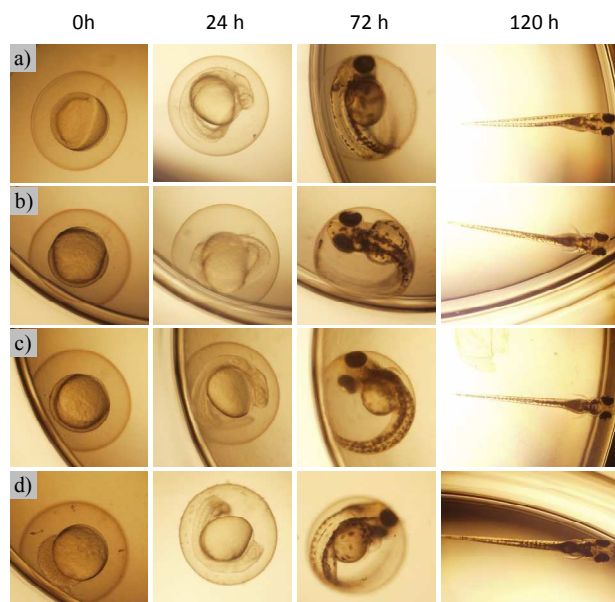
Figure 10. Embryo images of zebrafish exposed to varied concentration of CCM, namely 0 mg/mL as control (a), 0.14 mg/mL (b), 0.7 mg/mL, and 1.4 mg/mL (d). Oxygenated water was used as solvent for diluting CCM.
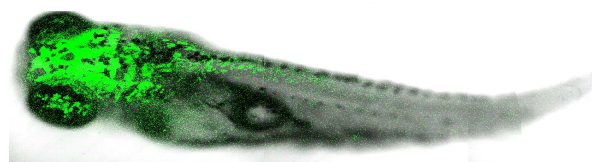

Figure 11. CLSM images of zebrafish at 488 nm excitation wavelength. Green colour signal form the emission of CCM.

4. Conclusion

We have developed a facile method for the ultrasonic-assisted phase transfer of MnFe$_2$O$_4$ MNPs from organic solvents to aqueous solutions using CBBA capping ligand. This process generates well-dispersed, water-soluble MNPs that have phenylboronic acid groups on the surface. The phenylboronic acid groups can be used as targeting ligands and for conjugation to fluorescent Cdots, resulting in the formation of phenylboronic acid-modified magnetofluorescent NPs. The NPs show moderate stability in physiological conditions, and no cytotoxicity was observed *in vitro* (HeLa cells) or *in vivo* (zebrafish embryos) over a range of concentrations. Our results indicated that magnetofluorescent NPs are effective contrast agents in T$_2$-weighted MRI and could be used for *in vitro* or *in vivo* optical bioimaging applications. Additionally, a chemotherapy drug, Dox, was loaded onto the phenylboronic acid-modified magnetofluorescent NPs, and released in a controlled manner at low pH values; this enabled the successful inhibition of HeLa cell proliferation. The above results demonstrated that our NPs have potential as effective dual-modality molecular imaging probes and drug delivery agents for simultaneous cancer diagnosis and chemotherapy.

Competing interests:

The authors have declared that no competing interest exists.

Reference

(1) J. Cheon and J. -H. Lee, *Accounts Chem. Soc.*, 2008, **41**, 1630–1640

(2) D. Shi, N. M. Bedford and H. -S. Cho, *Small*, 2011, **7**, 2549–2567.

(3) D. -E. Lee, H. Koo, I. -C. Sun, J. H. Ryu, K. Kim and I. C. Kwon, *Chem. Soc. Rev.*, 2012, **41**, 2656–2672.

(4) J. -C. Hsu, C. -C. Huang, K. -L. Ou, N. Lu, F. -D. Mai, J. -K. Chen and J. -Y. Chang, *J. Mater. Chem.*, 2011, **21**, 19257–19266.

(5) C. -Y. Cheng, K. -L. Ou, W. -T. Huang, J. -K. Chen, J. -Y. Chang and C. -H. Yang, *ACS Appl. Mater. Interfaces*, 2013, **5**, 4389–4400.

(6) C. -L. Huang, C. -C. Huang, F. -D. Mai, C. -L. Yen, S. -H. Tzing, H. -T. Hsieh, Y. -C. Ling and J. -Y. Chang, *J. Mater. Chem. B*, 2015, **3**, 651–664.

(7) M. Z. Fahmi, K. -L. Ou, J. -K. Chen, M. -H. Ho, S. -H. Tzing and J. -Y. Chang, *RSC Adv.*, 2014, **4**, 32762–32772.

(8) N. Lee and T. Hyeon, *Chem. Soc. Rev.*, 2012, **41**, 2575–2589.

(9) M. H. Pablico-Lansigan, S. F. Situ and A. C. S. Samia, *Nanoscale*, 2013, **5**, 4040–4055.

(10) H. Li, Z. Kang, Y. Liu and S.-T. Lee, *J. Mater. Chem.*, 2012, **22**, 24230–24253.

(11) P. G. Luo, S. Sahu, S. -T. Yang, S. K. Sonkar, J. Wang, H. Wang, G. E. LeCroy, L. Cao and Y. -P. Sun, *J. Mater. Chem. B*, 2013, **1**, 2116–2127.

(12) S. K. Bhunia, A. Saha, A. R. Maity, S. C. Ray and N. R. Jana, *Scientific reports*, 2013, **3**, 1473.

(13) S. Y. Lim, W. Shen and Z. Gao, *Chem. Soc. Rev.*, 2015, **44**, 362–381.

(14) S. D. Bull, M. G. Davidson, J. M. H. van den Elsen, J. S. Fossey, A. T. A. Jenkins, Y.-B. Jiang, Y. Kubo, F. Marken, K. Sakurai, J. Zhao and T. D. James, *Accounts Chem. Soc.*, 2012, **46**, 312–326.

(15) Z. Guo, I. Shin and J. Yoon, *Chem. Commun.*, 2012, **48**, 5956–5967.

(16) A. Liu, S. Peng, J. C. Soo, M. Kung, P. Chen and H. Duan, *Anal. Chem.*, 2011, **83**, 1124–1130.

(17) J. Balzarini, *Nat. Rev. Microbiol*. 2007, **5**, 583−597.·

(18) P. C. Trippier, J. Balzarini, C. McGuigan, *Antiviral Chem. Chemother*. 2011, **21**, 129−142.·

(19) Y. Dong, J. Shao, C. Chen, H. Li, R. Wang, Y. Chi, X. Lin and G. Chen, *Carbon*, 2012, **50**, 4738–4743.

(20) Q. Zhang, W. Li, T. Kong, R. Su, N. Li, Q. Song, M. Tang, L. Liu and G. Cheng, *Carbon*, 2013, **51**, 164–172.

(21) S. -Y. Lee and M. T. Harris, *J. Colloid Interface Sci.*, 2006, **293**, 401–408.

(22) A. -H. Lu, E. L. Salabas and F. Schüth, *Angew. Chem. Inter. Ed.*, 2007, **46**, 1222–1244.

(23) Z. Xu, C. Shen, Y. Hou, H. Gao and S. Sun, *Chem. Mater.*, 2009, **21**, 1778–1780.

(24) X. Wang, R. D. Tilley and J. J. Watkins, *Langmuir*, 2014, **30**, 1514–1521.

(25) R. Sondjaja, T. Alan Hatton and M. K. C. Tam, *J. Magn. Magn. Mater.*, 2009, **321**, 2393–2397.

(26) Y. Liu, T. C. Hughes, B. W. Muir, L. J. Waddington, T. R. Gengenbach, C. D. Easton, T. M. Hinton, B. A. Moffat, X. Hao and J. Qiu, *Biomaterials*, 2014, **35**, 378–386.

(27) D. Schmaljohann, *Adv. Drug Deliv. Rev.*, 2006, **58**, 1655–1670.

(28) S. K. Das, Y. Liu, S. Yeom, D. Y. Kim and C. I. Richards, *Nano Lett.*, 2014, **14**, 620–625.

(29) G. Eda, Y.-Y. Lin, C. Mattevi, H. Yamaguchi, H.-A. Chen, I. S. Chen, C.-W. Chen and M. Chhowalla, *Adv. Mater.*, 2010, **22**, 505–509.

(30) H. Chen, G. D. Wang, W. Tang, T. Todd, Z. Zhen, C. Tsang, K. Hekmatyar, T. Cowger, R. B. Hubbard, W. Zhang, J. Stickney, B. Shen and J. Xie, *Adv. Mater.*, 2014, **26**, 6761–6766.

(31) F. Wang, S. Pang, L. Wang, Q. Li, M. Kreiter and C. -Y. Liu, *Chem. Mater.*, 2010, **22**, 4528–4530.

(32) X. Wen, P. Yu, Y. R. Toh, X. Ma and J. Tang, *Chem. Commun.*, 2014, **50**, 4703–4706.

(33) A. B. Bourlinos, A. Stassinopoulos, D. Anglos, R. Zboril, M. Karakassides and E. P. Giannelis, *Small*, 2008, **4**, 455–458.

(34) H. B. Bosmann, A. Hagopian and E. H. Eylar, *Arch. Biochem. Biophys.*, 1968, **128**, 51-69.

(35) L. K. Mahal, K. J. Yarema and C. R. Bertozzi, *Science*, 1997, **276**, 1125-1128.

(36) J. A. Key, C. Li and C. W. Cairo, *Bioconjugate Chem.*, 2012, **23**, 363–371.

(37) K. Kostarelos, L. Lacerda, G. Pastorin, W. Wu, S. Wieckowski, J. Luangsivilay, S. Godefroy, D. Pantarotto, J. P. Briand, S. Muller, M. Prato and A. Bianco, *Nat. Nanotechnol.*, 2007, **2**, 108–113. □

(38) B. Chen, Q. Liu, Y. Zhang, L. Xu and X. Fang, *Langmuir*, 2008, **24**, 11866–11871.

(39) W. Shang, X. Zhang, M. Zhang, Z. Fan, Y. Sun, M. Han and L. Fan, *Nanoscale*, 2014, **7**, 5799–5806.

(40) L. Chen, L. Li, L. Zhang, S. Xing, T. Wang, Y. A. Wang, C. Wang and Z. Su, *ACS Appl. Mater. Interfaces*, 2013, **5**, 7282–7290.

(41) S. L. Harper, J. L. Carriere, J. M. Miller, J. E. Hutchison, B. L. S. Maddux and R. L. Tanguay, *ACS Nano*, 2011, **5**, 4688–4697.

(42) K. Kim and R. L. Tanguay, *Green Chem.*, 2013, **15**, 872–880.

(43) G. H. Jang, M. P. Hwang, S. Y. Kim, H. S. Jang and K. H. Lee, *Biomaterials*, 2014, **35**, 440–449.

Graphical abstract
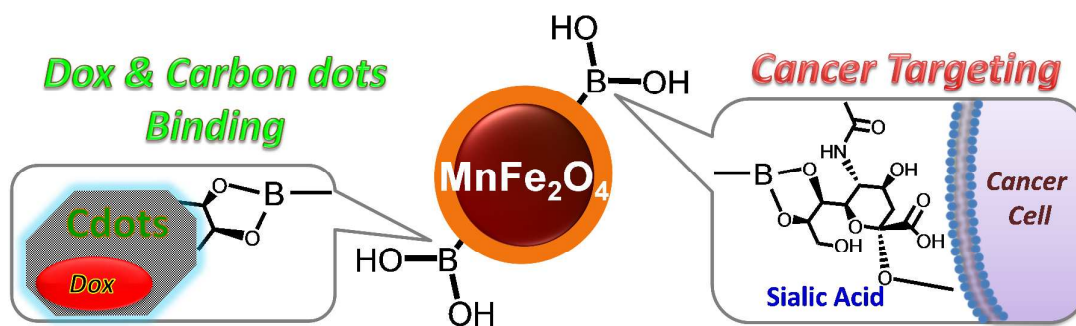
This paper reports the development of multifunctional nanoparticles as effective dual-modality molecular imaging probes and drug delivery agents for simultaneous cancer diagnosis and chemotherapy.